Rapid-Manufacturable Hair Sensor Array for Legged Millirobots

Jaakko T. Karras, Duncan W. Haldane and Ronald S. Fearing

Abstract— **We present a rapid-manufacturable, hair-actuated contact sensor array designed for use on legged millirobots. The sensor is an array of sensitive contact switches. Each switch is activated by loading a hair mounted at the switch tip. The hair sensor array is sufficiently sensitive to detect the small contact forces experienced by a lightweight robot, with an average normal sensitivity of 0.8 grams/hair. The compliant polymer hairs detect both normal and shear contact, allowing the array to detect a variety of contact forces. By virtue of its design, the hair sensor array can be fabricated using a roll-to-roll layered process. We demonstrate a straightforward application of the sensor technology on a hexapedal millirobot, using the array to both estimate average ground speed and detect high-centering when running over obstacles. This application is of particular interest for milliscale robots operating in rough terrain, where the risk of entrapment is high. Our results indicate that the hair sensor array can estimate ground speed and detect high-centering when running over simple geometric obstacles.**

I. INTRODUCTION

Legged millirobots, like the biological organisms that they mimic, can readily adapt to a variety of complex environments. These robots can operate in rough terrain, confined spaces, and in the presence of obstacles such as foliage. This versatility makes legged millirobots an ideal solution to tasks requiring high maneuverability in difficult and uncertain environments. Examples might include searching through wreckage in the aftermath of natural disasters, or performing inspection and maintenance tasks within the interiors of buildings and other structures. Ideally, many of these tasks would be completed either autonomously or semi-autonomously, allowing human operators to focus on higher-level organization and control. In order to operate effectively without constant human guidance, legged millirobots must be equipped with adequate sensing capabilities to characterize and respond to their surroundings.

Vision and sonar systems could provide a piece of the needed functionality by detecting environmental features at a distance, and would likely play a role in any autonomous millirobot. A semi- or fully-autonomous millirobot would, however, also require reliable information regarding its immediate surroundings, particularly about surfaces that it contacts. To be effective, especially in dark, highly confined spaces, an autonomously-operating millirobot needs reliable contact sensing such as that provided by antennae or distributed tactile sensors.

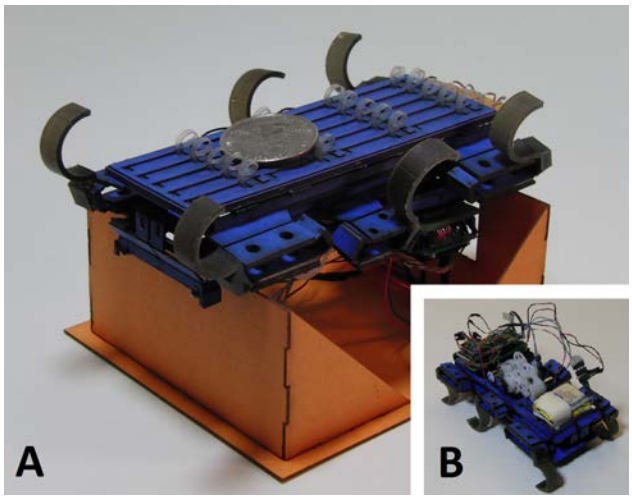

Fig. 1. (A) Hair-activated 5 x 4 contact sensor array mounted on bottom of a hexapedal millirobot. The array is 35 mm by 101 mm (width by length) and weighs 5 g. U.S. Quarter shown depressing second column of hairs. Robot is shown inverted on a supporting stand. (B) Millirobot standing upright, with hair array mounted to bottom.

Biology presents numerous solutions to the tactile sensing problem through the myriad of tactile sensing structures found in insects and mammals, such as touch-sensitive skin, hairs, whiskers, and antennae. In nature, such structures serve a wide range of sensory functions and much work has been done in recreating them for applications in mobile robotics. Wall-following behaviors have been implemented in both wheeled and legged mobile robots using artificial antennae and whiskers [2], [10], [11], [12]. Passive whiskers have been added to mobile robots to detect and recognize obstacles [15], [16], [19], and extensive work has been done in using whisker structures to identify textures and terrain [3], [4], [5], [13], [17], [18]. All of these sensing structures share the commonality that they extend well beyond the body of the robot, detecting features that are a certain distance away. Important information can also be gained by sensing contact much closer to the body of the robot. For instance, short ground-facing whiskers were mounted around the feet of a quadrupedal robot to measure foot-ground interactions [6]. Additional applications for hair-length body contact sensors could include preventing damage from contact, tracking the propagation of obstacles along the body to infer forward progress, and avoiding terrain features that might lift the the robot's legs off the ground and cause loss of traction (high-centering). Each of these applications is of practical value to

This work is supported by the DARPA Maximum Mobility and Manipulation program. D.W. Haldane is supported by NSF IGERT grant DGE-0903711.

J.T. Karras and R.S. Fearing are with Department of Electrical Engineering and Computer Sciences, University of California, Berkeley, CA 94720, USA {jkarras, ronf}@eecs.berkeley.edu

D.W. Haldane is with Department of Mechanical Engineering, University of California, Berkeley dhaldane@berkeley.edu

millirobots operating in obstructed environments.

In this work, we present a low cost, rapid-manufacturable hair-based body contact sensor array (Fig. 1), designed to be compatible with lightweight, rapid-manufactured legged millirobots such as DASH [1], DynaRoACH [7], and OctoRoACH [14]. The sensor consists of a 5 x 4 (rows x columns) array of highly sensitive binary contact switches, where each switch is activated by a compliant polymer hair originating from the tip of the switch. These biomimetic hairs detect both shear and normal contact forces, enabling the sensor array to detect a wide range of body contacts. The compliance of the hairs also enables the sensor to conform to uneven surfaces, making it useful for robots operating in rough terrain. The hair sensor design is novel in that it can be fabricated using an entirely laminar roll-to-roll process that is compatible with the scaled Smart Composite Microstructures (SCM) fabrication methodology [8] used to build the millirobots mentioned above.

In addition to describing the hair sensor design and fabrication, we also demonstrate its usefulness in context of two simple terrain-sensing applications: estimating ground speed and detecting high-centering in a hexapedal millirobot traversing geometric obstacles. In both applications, the hair sensor array is used to detect variation in ground contact along the bottom of the robot.

II. HAIR-ACTIVATED CONTACT SENSOR ARRAY

The main objectives for the design of the hair sensor array were to achieve high sensitivity, to detect a wide range of body contacts, and to develop a sensor that can be produced using rapid roll-to-roll fabrication processes at low cost. These objectives are achieved using an array of switches, where each switch is activated by a curled, compliant hair mounted at the tip. Each switch activates a junction in a resistive row-column matrix, which is sampled element-wise by an embedded processor to determine the contact pattern on the sensor. The entire sensor is assembled from 13 thin layers of cardboard, copper, various polymers, and sheet adhesive through lamination and laser cutting. As configured for this paper, the hairs have an average normal sensitivity of approximately 0.8 grams/hair, but the sensor design and fabrication methodology can be readily adapted to produce hairs of different sensitivities.

A. Mechanical Design

The hair sensor consists of an array of SCM switch structures, where each switch is activated by the loading of a compliant polymer hair at its tip (Fig. 2).

1) Hair-Activated Levers: The switches themselves consist of a lever arm (B) of rigid structural material hinged at one end through a polymer flexure (C). For our sensor array, we used four-ply cardboard ($\approx$0.4 mm thick) as the structural material and 75 μm-thick PET film for the switch flexure hinges. Curled polymer hairs (A) are held in place at the tip of each switch lever by small blocks of cardboard that, together with adhesive, adhere the roots of the hairs to the lever tips. When the hairs are perturbed, either through normal or shear contact forces, the levers deflect downward, pivoting at their flexure hinges.

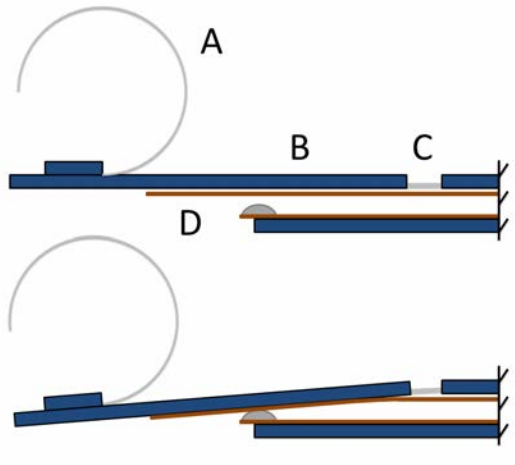

Fig. 2. Hair-based switch shown in both the open (top) and closed (bottom) configurations. Structure consists of a curled polymer hair (A), a rigid lever arm (B), a polymer flexure (C) and copper contacts (D).

2) Copper Contacts: The hair-lever structures sit above two copper contact layers (D), separated by a small air gap. When deflected by the hairs, the switch levers bring the top copper layer into contact with a rounded solder contact positioned at the end of the bottom copper layer. The top copper contacts form the sensor array columns, and the lower copper contacts form the rows. While it did not present significant problems during this work, oxidation can be reduced by gold-plating the copper layers prior to assembly, although at added cost. Alternatively, the copper contacts could be replaced entirely with analog transducers, such as capacitive or optical units, for an analog sensor array.

B. Electrical Design

The row and column conductors beneath each switch lever are part of a resistive array, with a resistor placed in series with each switch (Fig. 3). For our sensor, 10 kΩ resistors were soldered in series with each lower row contact. The resistors are needed to be able to localize the sources of contacts using the sampled electrical signals, since the absence of resistive elements at each junction would allow for cross-talk. Diodes could also be used, but we chose resistors since these can ultimately be replaced with resistive ink to avoid discrete components, further improving manufacturability.

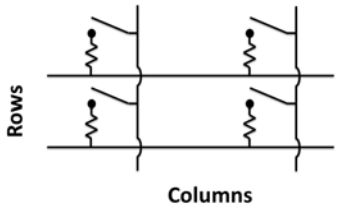

Fig. 3. Schematic illustrating two rows and two columns of a resistive array of hair switches.

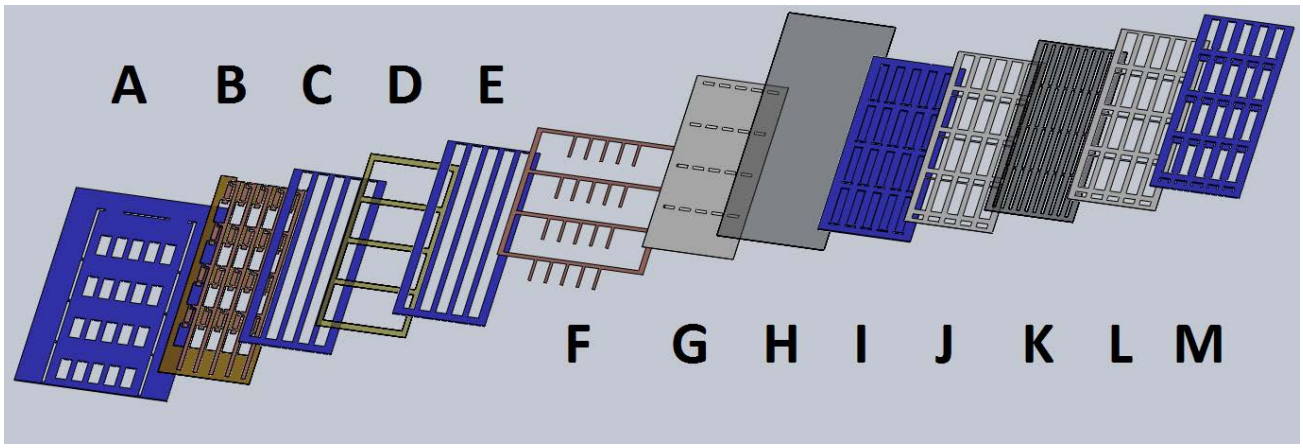

Fig. 4. Layers that comprise the hair sensor array: (A) Base Layer (B) Bottom Contacts (C) Spacer (D) Insulating Polymer Film (E) Spacer (F) Top Contacts (G) Paper Backing (H) Flexure Polymer Film (I) Switch Levers (J) Pre-Cut Sheet Adhesive (K) Pre-Stressed Hair Film (L) Pre-Cut Sheet Adhesive (M) Hair Mounting Layer. For visualization purposes, layers I and M are shown with laser-cut features that are actually formed after lamination.

C. Fabrication

One of the key design features of the hair sensor array is that it can be fabricated using an entirely laminar process, in which the full sensor is assembled by stacking up layers of material via lamination, while forming the required mechanical features on the accumulating stack-up using a laser-cutter. Overall, the hair sensor array is the product of 13 separate layers that stack together to form the electrical contacts, switch levers and hairs (Fig. 4). This process, which is detailed below, is also illustrated in the supplemental video for this paper.

1) Lower Half: Initially, the lower half of the sensor and the upper half with the hair-activated levers are built up independently, as two separate layered structures. The lower electrical contacts are formed by laminating a thin flex circuit (B) in between a rigid base layer (A) and a rigid spacer layer (C). The flex circuit contains the lower copper contacts and discrete resistors. An insulating polymer layer is then added (D), followed by another rigid spacer (E) to create a ≈1 mm gap between the flex circuit and the switch levers.

2) Upper Half: The mechanical top half of the sensor begins with the formation of the hinge flexures (H & I). This follows a process similar to that described in [8], with the exception that the flexure is only laminated to one rigid layer, not in between two, in order to keep the switch levers thin. A paper backing (G) is laminated to the underside of the levers to ensure that the electrical contact sides of the levers are uniform. The levers are then partially freed from the structure via laser-cutting. The levers are left partly connected at this point so that the hairs (L) can be attached with the levers still stationary.

3) Polymer Hairs: The curled hairs consist of a composite of 25 μm polypropylene (PP) film laminated together with 50 μm low-density polyethylene (LDPE) film. When laminated at a temperature of 177 °C (350 °F) and a pressure of 345 kPa (50 psi), the two films fuse together and the composite PP-LDPE film curls into a roll with a radius of curvature of ≈3-4 mm. This pre-curled hair film is then laid out flat, cut via laser to free the sides of the individual hairs, and embedded in a pre-stressed, flattened state between the levers and another structural layer (M). Selectively-cut sheet adhesive layers (J & L) hold the roots of the hairs between the two rigid structures.

4) Final Cuts: With the pre-stressed hair film in place, the upper and lower half-structures are laminated together with the upper electrical contacts (F) placed in between the two. The hair switches are completed by two sets of laser cuts: one to fully free the levers and a second to free the tops of the embedded hairs, which immediately curl out of the plane of the sensor due to their being in a pre-stressed state prior to the final cuts (Fig. 5). The full sensor is completed by simply freeing it from the supporting structure around the base (A), and by cutting away the sides of the column conductor layer (F) to electrically isolate the columns.

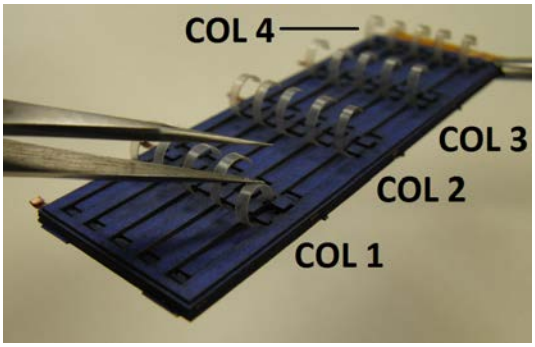

Fig. 5. Completed 5 x 4 hair sensor array.

D. Read-Out Electronics

In order to collect data from our hair sensor arrays, we designed a 20 mm (W) by 43 mm (L) printed circuit board with an embedded 16-bit dsPIC33F microcontroller and analog multiplexers. The electronics can scan the array at ≈2,000 samples per second for a frame rate of 100 Hz.

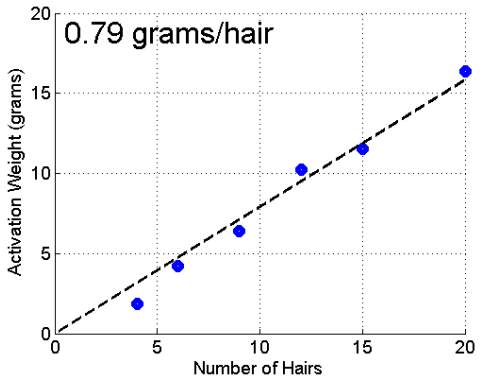

Fig. 6. Total loading required for sensor activation as a function of the number of hairs loaded.

E. Hair-Switch Sensitivity

The average sensitivity of the hair-switches in our 5 x 4 array was computed by determining the minimum threshold weight at which different sized patches of hairs become active. Here, a patch of hairs was labeled as active if at least 2/3 of the loaded hairs were active. The results of these trials are plotted in Fig. 6. The dashed trend line is the least-squares fit (zero intercept) to the data points, indicating an average normal sensitivity of 0.79 grams/hair.

III. CONTACT-BASED GROUND SPEED ESTIMATION

In order to test the hair sensor technology, we mounted a 5 x 4 hair array on the bottom of a hexapedal millirobot and used a pair of contact-sensing algorithms to detect high-centering and to estimate average ground speed when running over an obstacle. Both tasks are important problems when operating in rough terrain, where the high risk of entrapment requires that autonomous robots be able to reliably estimate their rates of forward progress and use that information to update their locomotive strategies when necessary.

A. Robot Design

We designed a new hexapedal millirobot (Fig. 1) to study the performance of the sensor on a dynamic platform. The locomotion system of the robot comprises the chassis, transmission and legs. Using the SCM Process [8] we fabricated a lightweight chassis and transmission that were rapidly optimized for compatibility with the sensor using an iterative design process. Unlike previous millirobots such as DASH [1] or DynaRoACH [7], this robot features a new chassis with a static bottom plate to facilitate integration for the tactile sensor. We maintained the proven feed-forward, alternating tripod gait kinematics of the DynaRoACH platform [7], but made several modifications. The nominal touchdown and liftoff angles of $\pm 42^{\circ}$ were kept and the duty cycle remained at 0.5. However, we split the transmission down the sagittal plane, using one motor per side to drive two independent sets of three legs each. This split transmission enables robust steering control [14]. Dynamic simulations predict that running on curved legs expands the region of stable running [9], a conclusion substantiated by the performance of the highly dynamic modern RHex family of robots, which utilize semicircular C shaped legs. We cast semicircular legs for the robot using a polyurethane elastomer (PMC-790 Smooth-On, Inc.). Parameters for the legs and the complete locomotion platform can be found in Table I.

TABLE I
PHYSICAL ROBOT PARAMETERS

Body Size	100 mm (L) 58 mm (W) 45 mm (H)
Total Mass	46.7 g (38.3 g without battery)
Leg Stiffness	$80\frac{N}{m}$
Leg Diameter	2.25 cm
Motors	2 x Didel MK07-3.3Ω
Gear Ratio	23.1:1

B. Sensor Integration

A 5 x 4 (rows by columns) hair sensor array was integrated with the experimental hexapedal millirobot. The sensor array was mounted against the bottom of the robot, hairs facing downward, with the rows oriented lengthwise along the robot, and the columns perpendicular to the direction of forward motion (Fig. 1).

C. Experimental Setup and Methods

Ground speed estimation data was collected by running the robot over a rectangular box (25 mm W, 20 mm L, 7 mm H) attached rigidly to a textured tile surface (Fig. 7). The robot was set to run directly over the the box at a variety of commanded speeds. The ground-facing sensor array was scanned at 100 Hz (100 full 5 x 4 frames per second), and the data logged to a Flash memory onboard the robot. Ground speed estimation was performed offline using the contact data collected during the data runs. All runs were carried out under an OptiTrack[1] motion capture system in order to obtain ground-truth position data for later comparison.

High-centering data was collected by replacing the rectangular box with a wedge, inclined at 7 degrees (Fig. 8). The wedge was designed such that the robot would become high-centered when run directly onto it. Again, contact data was collected at 100 Hz and stored in the onboard Flash memory during each run, and ground-truth was recorded using the motion capture system.

D. Estimation Algorithm

We approach both the high-centering detection and ground speed estimation tasks by monitoring the average activation profiles for the four sensor columns over time. As the millirobot runs over an obstacle, we expect the obstacle to register on each of the four columns, beginning with the leading column, followed by the second and so forth. For a single obstacle, each of the column activation profiles should contain a single pulse, lasting the duration that the obstacle was beneath the column. Because of the spatial separation

[1]NaturalPoint, Inc. OptiTrack: http://www.naturalpoint.com/optitrack/

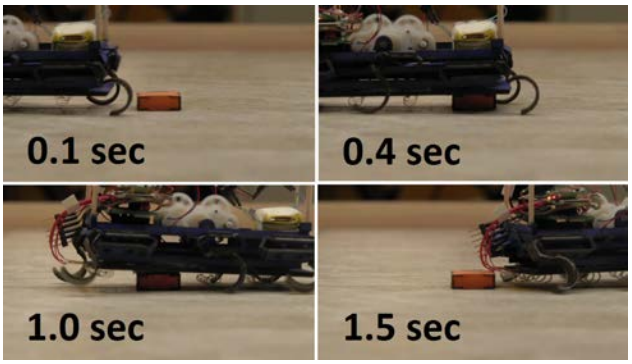

Fig. 7. Frames from video footage of hexapedal millirobot running over experimental block obstacle.

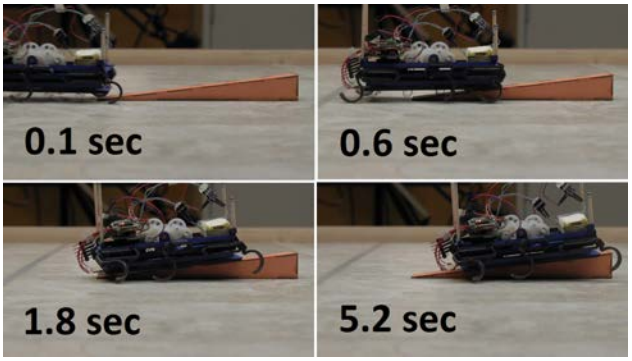

Fig. 8. Frames from video footage of hexapedal millirobot running onto high-centering wedge.

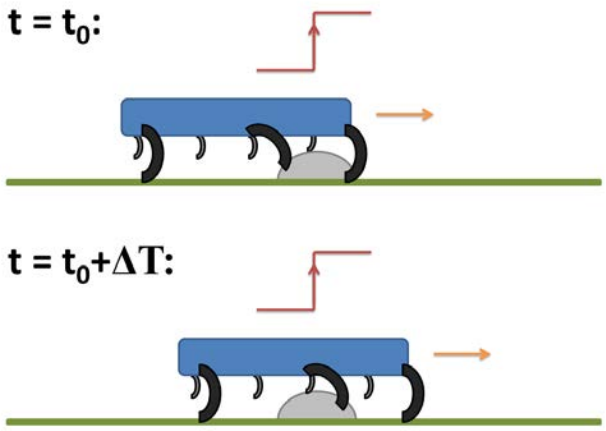

Fig. 9. An obstacle propagating down the length of a running hexapedal millirobot. A rising edge is first detected on the leading column (top) and a matching edge is detected on the next column a time ΔT later (bottom).

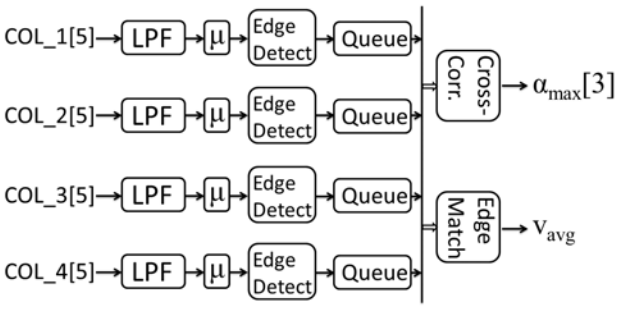

Fig. 10. A high-level block diagram of the algorithms used to detect high-centering and to estimate average ground speed.

between successive columns, there will be a time offset between the rising edge of the activation on one column and the same rising edge on the subsequent column. Knowing the distance between columns, we can estimate the average speed of the robot by matching edges (both rising and falling) across the sensor columns and recording the time delay between them (Fig. 9).

High-centering is detected by using the same column activation profiles and computing the pairwise maximum cross-correlation between the activation profiles of adjacent columns. In a forward-moving robot, the activation patterns of adjacent columns should show a high maximum cross-correlation value. This is because the peak cross-correlation value corresponds to the highest attainable degree of alignment between the two waveforms. As the robot becomes high-centered on an obstacle, however, the activation pattern corresponding to that obstacle will cease to propagate along the sensor array, resulting in poorly correlated activation profiles along the sensor. Thus, high-centering can be inferred when any of the pairwise correlations between adjacent columns drops beneath a minimum threshold.

Fig. 10 presents a block diagram of the contact-propagation algorithm. Sampled values from each of the four columns are passed through a low-pass filter (LPF block), after which they are averaged (μ block) to obtain a filtered mean activation for each column. These mean activation values are then passed into an edge detector, which applies thresholds to detect rising and falling edges. In the event that an edge is detected, it is stored in a queue of edges that can be referenced when edges are detected on the subsequent column. When matching edges are detected, the time delay between them is used to produce an estimate of the average ground speed. The activation waveforms encoded by the column edges are also correlated with one another in a pairwise fashion over a time window determined by the commanded speed, and the maximum value of each pairwise correlation is reported. If the maximum value of any pairwise correlation drops below a set threshold, the robot is inferred to be high-centered.

E. Results and Discussion

The results of a representative ground-speed estimation trial are plotted in Fig. 11. We observe from the column waveforms that the 7 mm tall obstacle produces a clear series of pulses along the columns of the sensor array as the robot crawls over it. As plotted, the first column (COL1) is the leading column at the front of the array. Because the obstacle propagates through all four columns, producing similar activation patterns for each column, the pairwise maximum correlation values between adjacent columns remain above the high-center detection threshold (0.05/1.0),

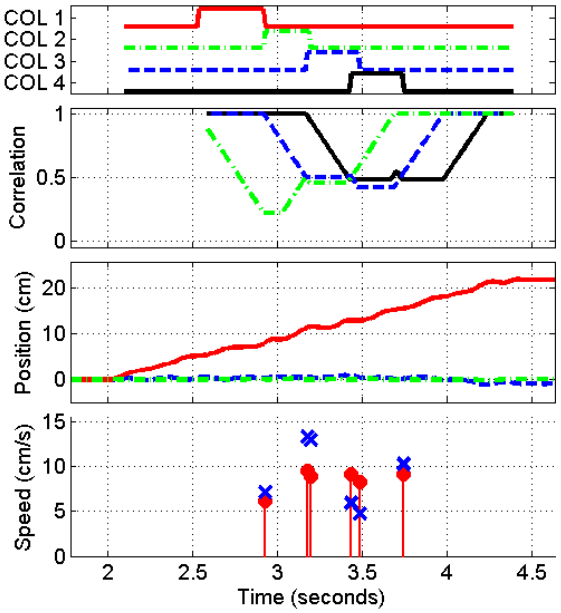

Fig. 11. A representative ground speed estimation trial. Column activation waveforms are plotted (top), followed by pairwise maximum correlations for adjacent columns. The correlation line styles match the waveforms that they correspond to. Column waveforms are always correlated with those from their leading neighbor. The first column is not correlated. Correlation plots are followed by ground-truth position curves. Lastly, average ground speed estimates (red circles) are plotted against true values (blue Xs) computed from the ground-truth data. All plots are time-synchronized.

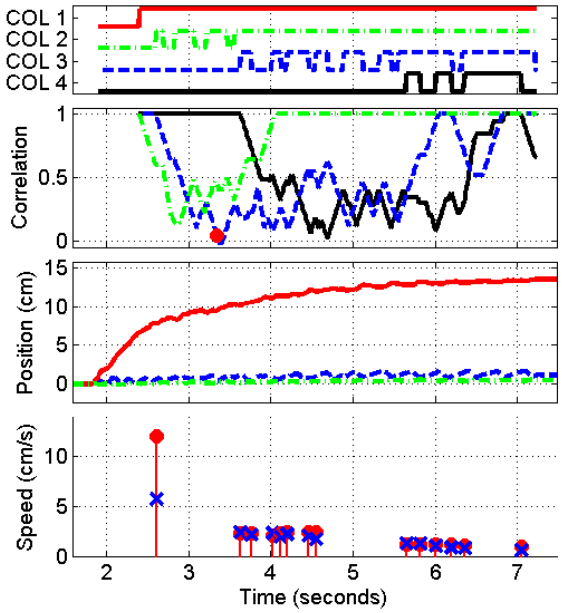

Fig. 12. A representative high-centering trial. The red circle in the correlation plot indicates the first point at which a maximum correlation value drops beneath a threshold of 0.05.

and high-centering is not a concern. The edge-matching algorithm detects each of the six matched edges (three rising, three falling), and estimates the average ground speed of the robot during the intervals between the matched edges. For the most part, the estimated average ground speeds follow the ground-truth speeds. For added reference, video of an example ground speed estimation trial is included in the video attachment.

Fig. 13 plots a collection of average ground speed estimates from a number speed estimation trials against their corresponding true average ground speeds, as determined from the motion capture data. The majority of the data points are clustered closely around the dashed $y = x$ line, indicating that the hair sensor array can reliably estimate the average ground speed from the 7 mm tall box when running over it at speeds up to about 10 cm/s. The data does reveal a few erroneous estimates, most of which are overestimates. In context of this experiment, the likeliest cause of these overestimates is that a column initially missed the edge of the obstacle, possibly due to the robot bouncing, resulting in the rising edge for the obstacle being detected late.

An example high-centering data set collected using the 7-degree wedge is shown in Fig. 12. As seen from the ground-truth position data, the forward progress of the robot levels off as it pushes its way onto the wedge. As this occurs, the first two columns of the sensor array transition into a permanently-on state, while the rear two columns begin to toggle as the rear legs, which retain ground contact, pitch the rear of the robot up and down. The edge propagation algorithm detects the dissimilarity between the columns, and infers that the robot has become high-centered once the maximum correlation between the second and third columns drops below the 0.05 minimum correlation threshold (red circle). An example high-centering trial can also be found in the companion video.

The correlation-based algorithm consistently detected high-centering when the robot was run onto the wedge with commanded speeds in the mid- to high range of speeds tested, an approximate distribution of which can be seen in Fig. 13. At these speeds, the algorithm detected high-centering in 93% of the wedge trials (15 trials). For comparison, the same algorithm produced false positives on 22% of the non-wedge trials conducted at the same speeds (18 trials).

IV. CONCLUSIONS AND FUTURE WORK

The hair-based contact sensor array presented in this paper provides a rapidly-manufacturable, low-cost contact sensing solution with sufficiently high sensitivity for use in legged millirobots. The hair-activated switch design has several key properties that make it particularly well-suited for our application. First, the switch lever arms provide mechanical amplification of contact forces, enabling the array to detect the small contact forces experienced by a millirobot. Second, the compliant hairs detect both the shear and normal components of contact forces and, by virtue of their compliance, enable the sensor array to conform to and detect uneven surfaces. This sensing versatility is crucial in

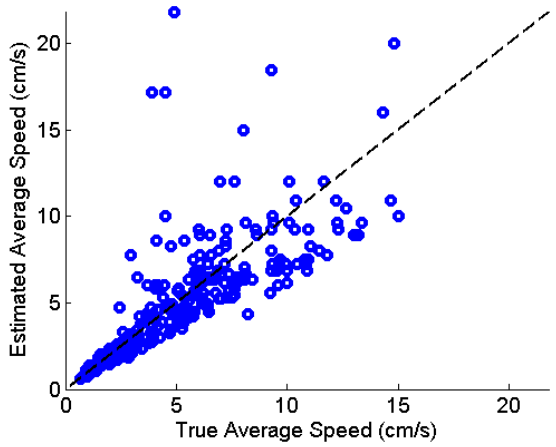

Fig. 13. A collection of average ground speed estimates plotted against their corresponding true average speeds. Plot contains 248 data points accumulated from 42 data runs. Dashed line represents y = x.

legged robots whose dynamics do not guarantee smooth or well-defined body contact patterns.

By virtue of its mechanical simplicity, the hair sensor array can be fabricated by incrementally laminating the component layers together and forming the required structures via laser-cutting. This ease of fabrication, combined with the hair array's flexible design, allow a handful of the sensor's properties to be easily tuned and tested for the desired application. The array dimensions, for instance, are easily modified by adding additional rows and columns to each layer of the sensor stack-up structure. Hair density can also be adjusted to achieve either more or less hairs per unit area. Hair sensitivity is easily adjusted by changing the lengths of the switch levers, the thickness of the flexure polymer, or the dimensions (length and width) of the flexures themselves.

The straightforward ground speed estimation and high-centering detection experiments demonstrate that the rapid-manufacturable hair array sensor can immediately begin to provide useful information about terrain interaction when running over simple obstacles. Using the hair sensor array, we reliably estimated ground speed up to speeds of roughly 10 cm/s when running over a single obstacle. Additionally, we were able to detect high-centering on a wedge over a range of commanded speeds. In future work, we hope to expand these results to more complex and realistic terrains by developing more robust algorithms and by enhancing the capabilities of the sensor itself.

ACKNOWLEDGMENT

The authors would like to thank Prof. Will Provancher (Univ. of Utah) for his input in the development of the hair sensor array, as well as the members of the U.C. Berkeley Biomimetic Millisystems Lab for their guidance and support.

REFERENCES

[1] P. Birkmeyer, K. Peterson, and R. Fearing, "DASH: A dynamic 16g hexapedal robot," in *IEEE/RSJ Int. Conf. on Intelligent Robots and Systems*, Oct 2009, pp. 2683 –2689.

[2] N. J. Cowan, E. J. Ma, M. Cutkosky, and R. J. Full, "A biologically inspired passive antenna for steering control of a running robot," in *Robotics Research*, ser. Springer Tracts in Advanced Robotics, P. Dario and R. Chatila, Eds. Springer Berlin / Heidelberg, 2005, vol. 15, pp. 541–550.

[3] M. Fend, S. Bovet, H. Yokoi, and R. Pfeifer, "An active artificial whisker array for texture discrimination," in *IEEE/RSJ Int. Conf. on Intelligent Robots and Systems*, vol. 2, Oct 2003, pp. 1044 – 1049 vol.2.

[4] M. Fend, "Whisker-based texture discrimination on a mobile robot," in *Advances in Artificial Life*, ser. Lecture Notes in Computer Science, M. Capcarrre, A. Freitas, P. Bentley, C. Johnson, and J. Timmis, Eds. Springer Berlin / Heidelberg, 2005, vol. 3630, pp. 302–311.

[5] C. Fox, B. Mitchinson, M. Pearson, A. Pipe, and T. Prescott, "Contact type dependency of texture classification in a whiskered mobile robot," *Autonomous Robots*, vol. 26, pp. 223–239, 2009.

[6] S. Hirose, S. Inoue, and K. Yoneda, "The whisker sensor and the transmission of multiple sensor signals," *Advanced Robotics*, vol. 4, no. 2, pp. 105 –117, 1990.

[7] A. Hoover, S. Burden, X.-Y. Fu, S. Sastry, and R. Fearing, "Bio-inspired design and dynamic maneuverability of a minimally actuated six-legged robot," in *IEEE RAS and EMBS Int. Conf. on Biomedical Robotics and Biomechatronics*, Sept 2010, pp. 869 –876.

[8] A. Hoover and R. Fearing, "Fast scale prototyping for folded millirobots," in *IEEE Int. Conf. on Robotics and Automation*, May 2008, pp. 886 –892.

[9] J. Y. Jun, D. Haldane, and J. E. Clark, "Compliant Leg Shape, Reduced-Order Models and Dynamic Running," in *International Symposium on Experimental Robotics*, 2010, pp. 1–15.

[10] D. Jung and A. Zelinsky, "Whisker based mobile robot navigation," in *IEEE/RSJ Int. Conf. on Intelligent Robots and Systems*, vol. 2, Nov 1996, pp. 497 –504 vol.2.

[11] A. Lamperski, O. Loh, B. Kutscher, and N. Cowan, "Dynamical wall following for a wheeled robot using a passive tactile sensor," in *IEEE Int. Conf. on Robotics and Automation*, April 2005, pp. 3838 – 3843.

[12] J. Lee, S. Sponberg, O. Loh, A. Lamperski, R. Full, and N. Cowan, "Templates and anchors for antenna-based wall following in cockroaches and robots," *Robotics, IEEE Transactions on*, vol. 24, no. 1, pp. 130 –143, Feb 2008.

[13] N. Lepora, M. Evans, C. Fox, M. Diamond, K. Gurney, and T. Prescott, "Naive bayes texture classification applied to whisker data from a moving robot," in *Int. Joint Conf. on Neural Networks (IJCNN)*, July 2010, pp. 1 –8.

[14] A. Pullin, N. Kohut, and D. Zarrouk, "Dynamic turning of 13 cm robot comparing tail and differential drive," in *IEEE Int. Conf. on Robotics and Automation*, May 2012.

[15] R. A. Russell and J. A. Wijaya, "Recognising and manipulating objects using data from a whisker sensor array," *Robotica*, vol. 23, no. 05, pp. 653–664, 2005. [Online]. Available: http://dx.doi.org/10.1017/S0263574704000748

[16] R. Russell and J. Wijaya, "Object location and recognition using whisker sensors," in *Australasian Conf. on Robotics and Automation*, Dec 2003.

[17] A. Schultz, J. Solomon, M. Peshkin, and M. Hartmann, "Multifunctional whisker arrays for distance detection, terrain mapping, and object feature extraction," in *IEEE Int. Conf. on Robotics and Automation*, April 2005, pp. 2588 – 2593.

[18] A. Seth, J. McKinstry, G. Edelman, and J. Krichmar, "Texture discrimination by an autonomous mobile brain-based device with whiskers," in *IEEE Int. Conf. on Robotics and Automation*, vol. 5, April 2004, pp. 4925 – 4930 Vol.5.

[19] J. Wijaya and R. Russell, "Object exploration using whisker sensors," in *Australasian Conf. on Robotics and Automation*, Nov 2002, pp. 180–185.